



# Numerical simulation on progressive failure of yielding support material for squeezing tunnel

Xiang Ci<sup>1</sup> · Xinyu Liu<sup>1,2</sup> · Xianjun Tan<sup>1</sup> · Diansen Yang<sup>1</sup> · Hongming Tian<sup>1</sup> · Weizhong Chen<sup>1</sup>

Received: 1 September 2023 / Revised: 10 October 2023 / Accepted: 22 October 2023 / Published online: 24 November 2023  
© Wrocław University of Science and Technology 2023

## Abstract

Yielding support is effective in controlling excessive deformation of soft rock in squeezing tunnel engineering, and the developed polyethylene (PE) pipe filled with foamed concrete is a good choice serving as a yielding support. To deal with distortions brought on by significant mesh deformations and to enhance visualization, a numerical simulation method based on finite element method-smoothed particle hydrodynamics coupling (FEM-SPH) is adopted taking into account the progressive failure of PE pipes filled with foamed concrete (FC-PE) during deformation. By simulating the gradual failure of foamed concrete through smooth particle flow and the wrapped PE pipe using the finite element method, the damage process of the filled pipe has been examined. Comparison with experimental results demonstrates the superiority of the proposed model in terms of computational efficiency and accuracy, investigating the impact of several critical variables on the energy absorption capabilities of FC-PE, as well as setting pertinent evaluation indicators based on practical engineering application conditions. Additionally, numerical results demonstrate that the frictional characteristics between PE pipe and foamed concrete have little effects on the deformation energy absorption properties. The numerical results also demonstrate that the FC-PE's diameter has a positive impact on both the energy absorption efficiency and the usage efficiency, while thicker FC-PE having a lower energy absorption efficiency.

**Keywords** PE pipes · Foamed concrete · FEM-SPH coupled simulation method · Progressive failure · Energy absorption

## 1 Introduction

High in situ stress or complex weak geological structures, such as phyllitic schist, argillaceous schist, clay, marl, slate, and tectonically altered gneiss, can cause large deformation when tunneling [22, 29, 30, 33]. According to Goel [12] and Xu et al. [35], tunneling in these soft rocks frequently causes asymmetry and time-dependent creep deformation, which can seriously destroy tunnel support systems. For instance, the Lanzhou-Xinjiang railway's Muzhailing [37] and Daliang [9] tunnels all experienced engineering catastrophes

brought on by significant soft rock deformations. The main hazards of the tunnels are shotcrete cracking, deformation of steel arches, and bottom bulging. The surrounding rock of the tunnel is primarily black schist and sandstone; the maximum convergence of the tunnel reached 1000 mm. Recently, the research focus has shifted to the “yielding supports” concept. Yielding support allows controlled rock deformation to reduce the stress of surrounding rock and support structure, thereby avoiding damage during the curing process of the shotcrete lining [3]. This concept addresses continuous time-dependent deformation. Numerous notoriously challenging tunnels, including the Jianzhong tunnel in China [38], the Enasan tunnel in Japan [16], the Lyon-Torino Base tunnel connecting Italy and France, the Tauern tunnel in Austria [24], and the Lyon-Torino Base tunnel connecting Italy and France [6], eventually adopted the yielding support to successfully address the tunnel squeezing issue. Cantieni and Anagnostou [7] proposed a compressible primary lining support technology in which numerous pre-deformed slots are set along the axial direction of the tunnel in the shotcrete lining and compressible units are installed. These units

✉ Xianjun Tan  
wzchen@whrsm.ac.cn

✉ Weizhong Chen  
xjtan@whrsm.ac.cn

<sup>1</sup> State Key Laboratory of Geomechanics and Geotechnical Engineering, Institute of Rock and Soil Mechanics, Chinese Academy of Sciences, Wuhan 430071, Hubei, China

<sup>2</sup> University of Chinese Academy of Sciences, Beijing 100049, China

have the advantages of low strength and high deformation capacity compared to the concrete lining and can absorb the deformation pressure of the surrounding rock, achieving the coordination of primary lining and surrounding rock deformation. Barla et al. [4] used various types of compressible units in compressible primary liners to establish compressible primary liners and carried out in practical engineering applications, which significantly increased the deformation capacity of the primary liners. Rodríguez and Díaz-Aguado [26] conducted a theoretical study on the support characteristics of compressible primary liners. Windsor and Thompson [32] proposed the idea of deformable anchors, which can deform along with the deformation of the surrounding rock and provide a stable anchorage force during the deformation process, thereby achieving coordinated deformation of the anchorage structure. He and Guo [13] developed a novel let-down anchor with negative Poisson's ratio material and thoroughly investigated its deformation properties. Based on taking into account the long-term time-dependent deformation of the surrounding rock, Chen et al. [8] proposed a cushioned let-load support method that can coordinate deformation with the surrounding rock and successfully applied it to the soft rock large deformation tunnel support. The compressible buffer layer can absorb the long-term deformation of the surrounding rock mass because it has a much higher deformation capacity than ordinary concrete, despite having a lower strength than concrete. Well, the buffer layer is typically positioned between the primary support and the secondary lining, thereby lowering the secondary lining's deformation pressure and ensuring the tunnel's operational safety. Due to its effective energy absorption, foamed concrete is recommended as a layer of protection. According to Amran et al. [2], foamed concrete benefits from a uniform hardening process during compression, a high strength-to-weight ratio, a low density, efficient construction, and ease of transport. Tan et al. [27] concluded that the foam concrete absorbed the majority of the energy released from the surrounding rock and proposed a combined supporting system based on foamed concrete as the main energy-absorbing material to resist large deformations in coal mine tunnels. Tian et al. [28] used polymeric foamed materials (polyurethane and polyethylene) as a compressible layer to lessen the secondary liner's vulnerability to compression damage caused by the surrounding rock. In order to evaluate and optimize the structural form of the energy absorber, Xiang et al. [34] proposed a number of key performance indicators. They came to the conclusion that filled tubes have better energy absorption performance than unfilled tubes and that round tubes have better energy absorption properties than square tubes. Baroutaji et al. [5] have conducted extensive research on thin-walled energy absorbers, comparing the loading results of thin-walled metal tubes with foam-filled tubes and concluding that the energy absorption effect of

filled tubes is significantly higher than that of thin-walled metal tubes. Laboratory experiments on polyethylene (PE) pipes filled with foamed concrete have shown its energy absorption behavior. However, there is lack of systematic and thorough numerical simulation on how PE pipes filled with foamed concrete fail during energy absorption, which is benefit for tunnel design on thickness of yielding support parameters.

Numerical simulation is a popular technique for simulating the progressive material damage processes in brittle materials like concrete and rock [10, 31, 36, 41]. These techniques include discrete element (DEM), coupled finite element-smooth particle flow, and coupled Eulerian–Lagrange computation. Although the finite element approach [39] can solve the stress, strain, and plasticity distribution of the structure in most cases, mesh distortion brought on by significant deformation makes it difficult to simulate crack expansion and material degradation. The discrete element approach [23] is frequently used in the simulation of granular aggregate materials and uses a rigid sphere (3D) or a rigid disc (2D) as the fundamental unit. The mechanical properties of materials like concrete and rock are described by defining the contact model and parameters between the fundamental units rather than the intrinsic model and parameters of the material. The peridynamics method [10] uses integral equations rather than partial differential equations to express the mechanical equations in order to solve the structural discontinuities that arise during crack extension and material damage. It discretizes the interested area into multiple material points, each of which is subject to the action of other material points and external loads.

Coupled Lagrange finite element and smooth particle hydrodynamic (FEM-SPH) numerical methods have been increasingly popular in recent years for simulating the gradual failure of composite materials. The reaction of a medium-strength rock under uniaxial compressive tests was studied by Mardalizad et al. [21], who also showed the accuracy of the coupled SPH and FEM methodologies in predicting crack development. The results demonstrated the effectiveness of the SPH method and the coupled FEM-SPH modeling technique in predicting the crushing behavior. Aktay et al. [1] used a meshless smooth particle hydrodynamic approach and a coupled FEM-SPH modeling technique to simulate the quasi-static axial crushing of polystyrene foam-filled aluminum thin-walled aluminum tubes. For the cases of a ball-tipped steel bullet impacting diagonally on a steel plate and a flat-tipped steel bullet impacting positively on a steel plate, Zhang et al. (2011) applied the concept of smooth kernel function deformation gradient and carried out three-dimensional numerical calculations using the coupled FEM-SPH contact algorithm. Dynamic compaction (DC) causes huge deformation

difficulties, and Wang et al. [29, 30] suggested a coupled FEM-SPH technique for analyzing these problems. They stated that the coupled FEM-SPH model might be a useful tool for analyzing large deformation problems in DC with greater accuracy and efficiency. Using the FEM-SPH approach, Gedikli [11] developed an improved design for foam-filled welded tubes (TWT). Actually, due to the large deformation of the FC-PE exposed to extrusion, smooth particle flow could be a useful technique to simulate the deforming, failure, and filling compactness of internally foamed concrete. Additionally, the external PE pipe was modeled using the finite element method (FEM) approach, which quickens the computation process and improves the correctness of the outcomes.

This study aims to conduct an in-depth simulation of the deformation and damage process of FC-PE by establishing a FEM-SPH numerical model and investigate the factors that affect the energy absorption characteristics of FC-PE and the influencing laws of each factor, thereby providing a basis for the application of FC-PE in tunnel yield support engineering. The outside-wrapped PE pipe was modeled using finite elements, and the foam concrete was modeled using smooth particles throughout the entire FEM-SPH model. To confirm the accuracy of the numerical model, the experimental results were compared with the numerical results of displacements and energy absorption. Then, a throughout analysis of FC-PE's deformation and damage process was performed based on the numerical simulation. Furthermore, numerical models for various sizes of FC-PE were established, and the load-bearing and energy-absorbing behavior were compared and optimized using the indicators of total energy absorption, specific energy absorption, effective displacement, and effective strain.

## 2 Materials testing

### 2.1 Testing of PE

Due to the temperature sensitivity of PE100, polyethylene pipe specimens were cut from PE100 grade pipes as indicated in Fig. 1, with a density of  $900 \text{ kg/m}^3$  and  $20 \text{ }^\circ\text{C}$  room temperature during the testing.

It may be deduced from prior research [18, 19, 25] that PE materials are isotropic and have side effects based on the processing features of PE and the material qualities. It was discovered that PE pipe exhibits the type of tensile damage because PE100 grade pipe is too thin to perform compression testing and from the experimental results of the foamed concrete-filled PE pipe [40]. Therefore, quasi-static tensile tests rather than quasi-static compression testing were applied. As seen in Fig. 2, the experiments were conducted on a micro-test double screw macroscopic tensile table. With

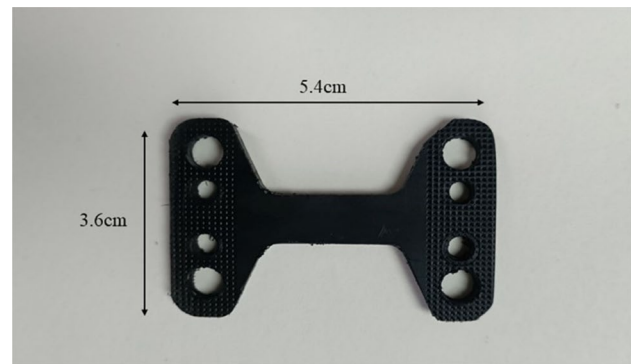


Fig. 1 Diagram of PE specimen

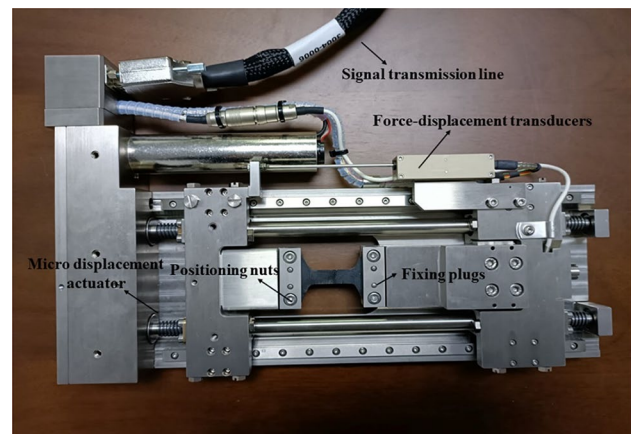


Fig. 2 Schematic of micro-test double screw macroscopic

a maximum load of 5 kN, this experimental apparatus is made to perform tensile testing on small objects. Experimental data are recorded using a load force transducer, which has a measurement precision of 50 N. The tensile test was performed on this experimental platform using flat specimens that were fastened using a flat fixture and double-positioning pins.

### 2.2 Constitutive model of PE

The quasi-static compression stress–strain curve for PE grade 100 was created by processing the data from the quasi-static tensile trials, as shown in Fig. 3. As seen, PE material exhibits a linear elastic behavior during the early stretching process before entering plasticity when the tensile strength exceeds 16 MPa and manifesting a plastic hardening behavior. The outcomes demonstrate the ductility of PE material and the absence of evident fissures during the plastic hardening step. The constitutive equation is constructed by describing the yield stress of PE as a function of the plastic

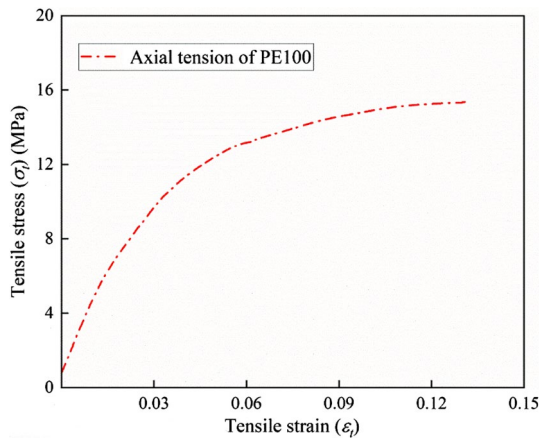


Fig. 3 Mechanical property curves of PE

strain, making PE material an appropriate plastic hardening material.

### 3 Numerical simulation on failure process of PE pipes filled with foamed concrete

#### 3.1 Numerical method of FEM-SPH

To assure the accuracy and efficiency of the computation while offering a realistic response to the deformation and stress distribution of the PE pipes filled with foamed concrete, a coupled FEM-SPH numerical calculation approach was used in this study. The technique employs smooth particle flow in the high-distortion region and FEM mesh cells in the low-distortion region. Smooth particles are formed when the foamed concrete satisfies a predetermined failure criterion, and they inherit the material parameters, mechanical properties, and energy accumulation previously set. The coupled FEM-SPH algorithm ensures computational accuracy and boosts calculation speed by taking into account both the continuity and discontinuity of the composite material as well as the transition of foamed concrete from a continuous medium to a discontinuity [14, 15, 20].

SPH method which represents the state of a system through a set of particles is quite suitable for simulating large deformation phenomena. These particles hold material properties and interact with each other over a range of dimensions. They are controlled by a smoothing (kernel) function. The kernel is determined for any two given particles,  $i$  and  $j$ , whose core approximation is as follows:

$$f(x_i) = \int_{\Omega} f(x_j)W(x_i - x_j, h)dx_j, \tag{1}$$

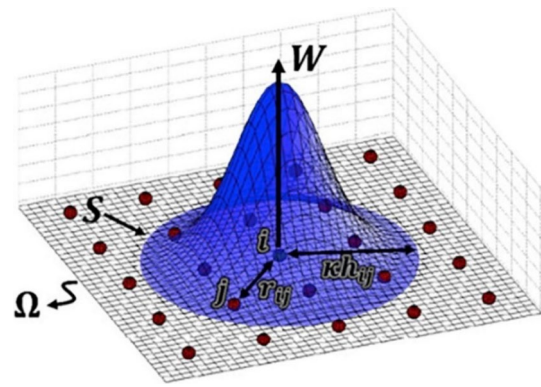


Fig. 4 SPH particles in a two-dimensional problem domain [21]

where  $x_i$  and  $x_j$  are the projected coordinates of the coordinate field of the particle in the problem domain,  $h$  is the distance between the two particles, and  $W$  is the smoothing function as follows:

$$W(x_i - x_j, h) = \frac{1}{h(x_i - x_j)^d} \theta(x_i - x_j), \tag{2}$$

where  $d$  is the spatial dimension and  $\theta$  is the auxiliary function. Figure 4 illustrates the principle of the SPH method. As connectivity between particles is considered a part of the computational process, extreme deformations can be directly dealt with by implementing the SPH method.

#### 3.2 Constitutive model of foamed concrete

The crushable foam model is often used to describe structures as energy absorbers. Foamed concrete has a high deformation and strong energy absorption capacity and can therefore be modeled to express its mechanical properties. The yield surface of the constitutive model is an ellipse on the meridian and can be expressed by the following equation:

$$F = \sqrt{q^2 + \alpha^2(p - p_0)^2} - B = 0, \tag{3}$$

$$\alpha = \frac{B}{A}, \tag{4}$$

$$p_0 = \frac{p_c - p_t}{2}, \tag{5}$$

where  $p$  is the mean stress,  $q$  is the Mises stress,  $\alpha$  is the shape factor,  $A$  and  $B$  represent the long and short axes of the elliptical yield surface on the meridian, respectively,  $p_0$  is the center on the yield ellipse, and  $p_t$  and  $p_c$  are the yield strengths for hydrostatic tension, respectively. Since hydrostatic and tensile tests are difficult to carry out on the material splash foam concrete and the choice of tensile

strength should not have a significant influence on the numerical simulations, the uniaxial yield strength  $s$  is used to approximate the above parameters as follows:

$$p_c = \frac{1}{k} \sigma_c, \tag{6}$$

$$p_t = \frac{k_t}{k} \sigma_c, \tag{7}$$

$$\alpha = \frac{3k}{\sqrt{(3k_t + k)(3 - k)}}, \tag{8}$$

where  $k$  and  $k_t$  are input parameters in the crushable foam and the values were determined to be 0.567 and 0.1, respectively, according to the documentation of ABAQUS.

The platform stage and densification stage of the stress–strain curve for foamed concrete are expressed as a volume-hardening function of the crushable foam. Since the yield surface evolves in a self-similar manner ( $\alpha$  remains constant), the plastic strain has no effect on  $p_t$ . The stress  $p_c$  can be written as follows:

$$p_c(\epsilon_{vol}^{pl}) = \frac{\sigma_c(\epsilon_{vol}^{pl}) \left[ \sigma_c(\epsilon_{vol}^{pl}) \left( \frac{1}{\alpha^2} + \frac{1}{9} \right) + \frac{p_t}{3} \right]}{p_t + \frac{\sigma_c(\epsilon_{vol}^{pl})}{3}}. \tag{9}$$

### 3.3 Numerical modeling based on FEM-SPH

The lateral quasi-static compression process of the PE pipes filled with foamed concrete (FC-PE) was modeled in three dimensions using ABAQUS software in conjunction with specified experimental process parameters. The PE pipe has

a 100 mm length, a 50 mm exterior diameter, and a 3 mm thickness, as shown in Fig. 5. Foam concrete has a diameter and length of 44 and 100 mm, respectively. Foam concrete and PE pipe both have the element types C3D8 and C3D8R, respectively. The FC-PE’s material properties were set as stated in Table 1. The tangential and normal contact qualities of PE pipe and foam concrete were determined to be, respectively, a penalty method with a frictional coefficient of 0.5 and a hard contact method.

The upper and lower loading plates are both 200 mm long and 100 mm wide. Both loading plates were created using the S4R element and have rigid shell bodies. The penalty method and hard contact method were also chosen as the contact property between loading plates and PE pipe, but the frictional coefficient was 0.2.

A conversion command was used to turn the foam concrete elements into smooth particles before analysis began, and three particles were allocated to a single C3D8R element. The lower plate remained fixed the entire time, while the upper plate went downward at a steady pace of 0.1 mm/s that was consistent with the test loading speed. When the proportion of upper plate vertical displacement to PE pipe exterior diameter (i.e., nominal strain) reached 70%, the analysis was considered complete.

**Table 1** Materials parameters and constitutive model

Materials	Density (kg/m <sup>3</sup> )	Elastic modulus (MPa)	Poisson’s ratio	Constitutive model
PE	900	250	0.3	Plastic hardening
FC	600	300	0.25	Crushable foam

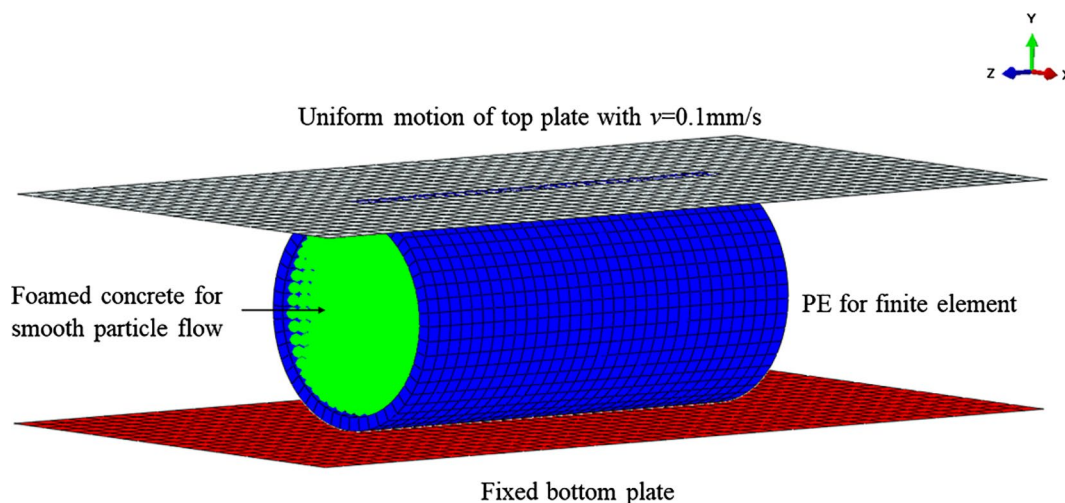


**Fig. 5** Coupled FEM-SPH modeling of FC-PE

## 4 Numerical results and discussion

### 4.1 Comparison between experimental and numerical results

In Fig. 6, the relationship curves between vertical displacement and load from the experiment and FEM-SPH numerical simulations are presented and contrasted with the results of the experiment. The simulation results are comparable to the experimental data in that they likewise clearly demonstrate the three stages of the load–displacement curve: elastic, plastic, and dense.

The relationship curve evolves in a non-linear elastic trend in the initial stage. The foamed concrete has not yet manifested apparent distortion and damage, and the PE pipe is still in an elastic state when the contact between the foamed concrete and PE is continually tightened. The connection curve tends to level off in the second stage. At this stage, foamed concrete experiences significant strain rates because a portion of it is plastic and potentially unstable. Due to the high porosity of foamed concrete, the internal gaps are regularly filled with shattered concrete debris, and PE pipe is positioned closer to pressure-wrapped foamed concrete, preventing the curve from reaching the platform stage completely. Instead, a smaller slope is continuously developing. The foamed concrete in the third stage, often known as the dense portion, approaches the total collapse as the nominal strain exceeds 0.6, and the shattered concrete debris entirely fills the interior spaces. The reason for the sharp rise in the curve mainly comes from two aspects. The PE pipe's confinement causes the broken foamed concrete to be compressed into a new whole, on the one hand, and on the other hand, the original concentrated load was transformed into a uniformly distributed load due to the significant

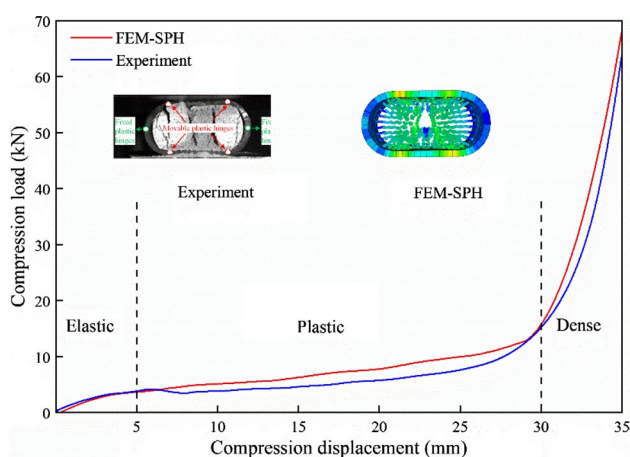


**Fig. 6** Comparison of simulation results on lateral compression of PC-PE with experimental results

deformation of PE pipe. At this time, PC-FE is equivalent to a plate subjected to unidirectional compressive load in the thickness direction, with a significant increase in stiffness compared to the elastic and plastic stages.

The total energy absorption (TEA) indicator is used to evaluate energy absorption property of FC-PE, which is defined as follows:

$$TEA = \int_0^s F(s)ds. \quad (10)$$

According to Eq. (10), the area enclosed by the vertical load–displacement relationship curve and the  $X$ -axis is numerically equal to the total absorbed energy. The TEA error between experimental and numerical results is less than 10%, as shown in Fig. 7. The difference between experimental and numerical results for the maximum reaction force is less than 6%. Errors are typically caused by two factors. Firstly, in contrast to numerical simulation, it was challenging to guarantee that the pouring and vibrating were homogeneous during the experimental process, leading to a problem with the specimen's non-homogeneity. Secondly, during extrusion, foamed concrete that is not axially restrained flows out of the ports on both sides, and the experimental process curve's plastic phase is smoother due to the overall decrease in compression volume.

In conclusion, the coupled FEM-SPH numerical technique demonstrates the effectiveness of FEM-SPH in simulating the lateral compression of quasi-static PE pipes filled with foamed concrete by ensuring the accuracy of the calculation results and outlining the entire failure process of FC-PE.

### 4.2 Results of the deformation and damage process of FC-PE

Figures 8 and 9 depict the stress changes and plastic zone changes of the foamed concrete throughout the entire quasi-static lateral compression of FC-PE process. In order to better understand the large deformation and damage process, the smooth particle flow illustration is used here.

Due to the influence of the pressure head, the foamed concrete will experience its greatest stresses at the top and bottom during the initial elastic phases (a) and (b). Due to the PE pipe's lack of constraint, the foamed concrete at the left and right ends moves to the sides as the contact area between the pressure head and the pipe expands. At the top and bottom, the plastic foamed concrete is partially broken before filling the core. At this phase, the stress of foam concrete is similar to the splitting test of concrete, and there is tensile stress inside.

**Fig. 7** Computation of absorbed energy during lateral compression of PC-PE

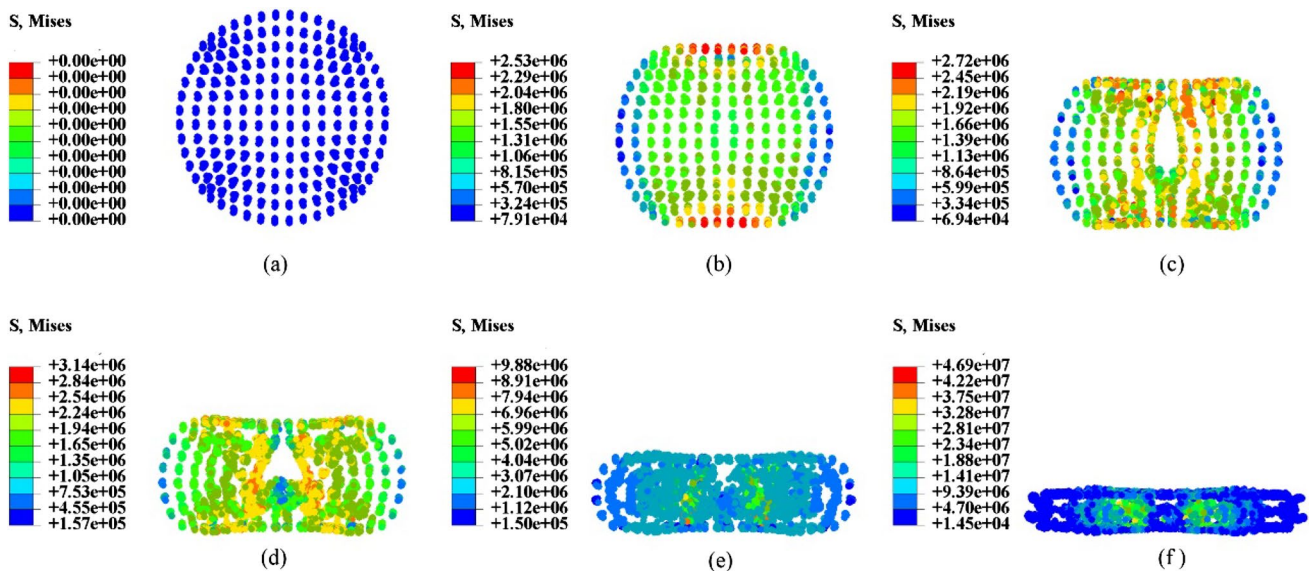
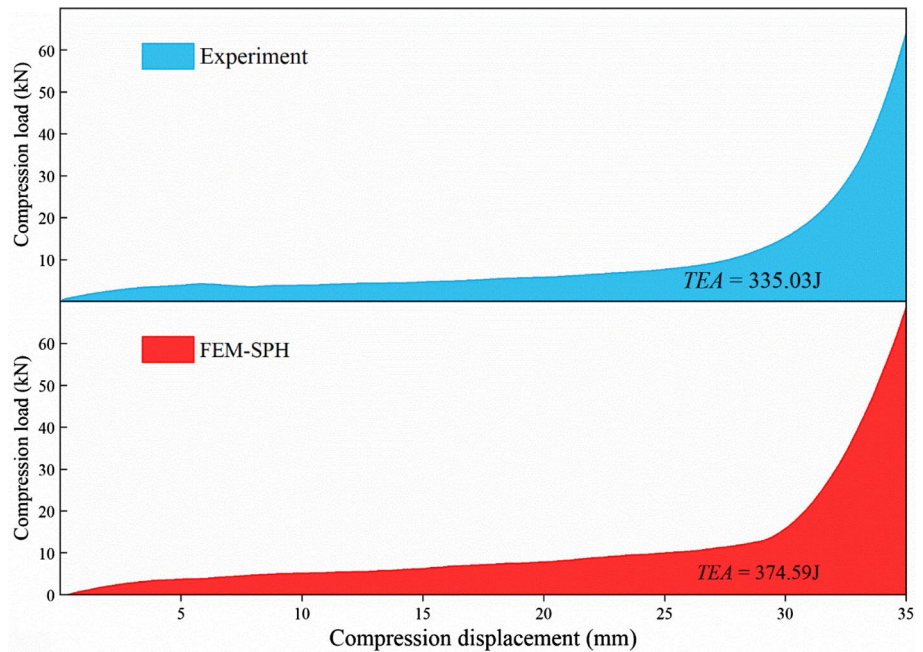


**Fig. 8** Distribution of Mises stress with different compression displacements. **a**  $s=0$  mm; **b**  $s=7$  mm; **c**  $s=14$  mm; **d**  $s=21$  mm; **e**  $s=28$  mm; and **f**  $s=35$  mm

When the external load exceeds a certain value, the internal tensile stress of the concrete will reach its tensile strength, resulting in cracks. Due to the PE pipe’s deformation during the elastic–plastic phase (c), the top and bottom of the PE will bulge, which will cause the upper and lower ends of the foamed concrete to further extrude. As a result, the shear stress causes the plastic zone to gradually spread to the concrete’s core, and the foamed concrete exhibits an X-shaped damage form. Vertical tensile cracks

are produced as the core of the concrete particles in the vertical direction move to the sides.

Under the wrapping effect of the PE pipe, foamed concrete was unable to expand freely in the core area of crack propagation and coalescence. Gravity and top pressure caused the broken concrete in the upper end to move downward, while the broken concrete in the lower end moved upward to fill the pores in the core zone (d). The broken concrete keeps moving to both sides as the pressure

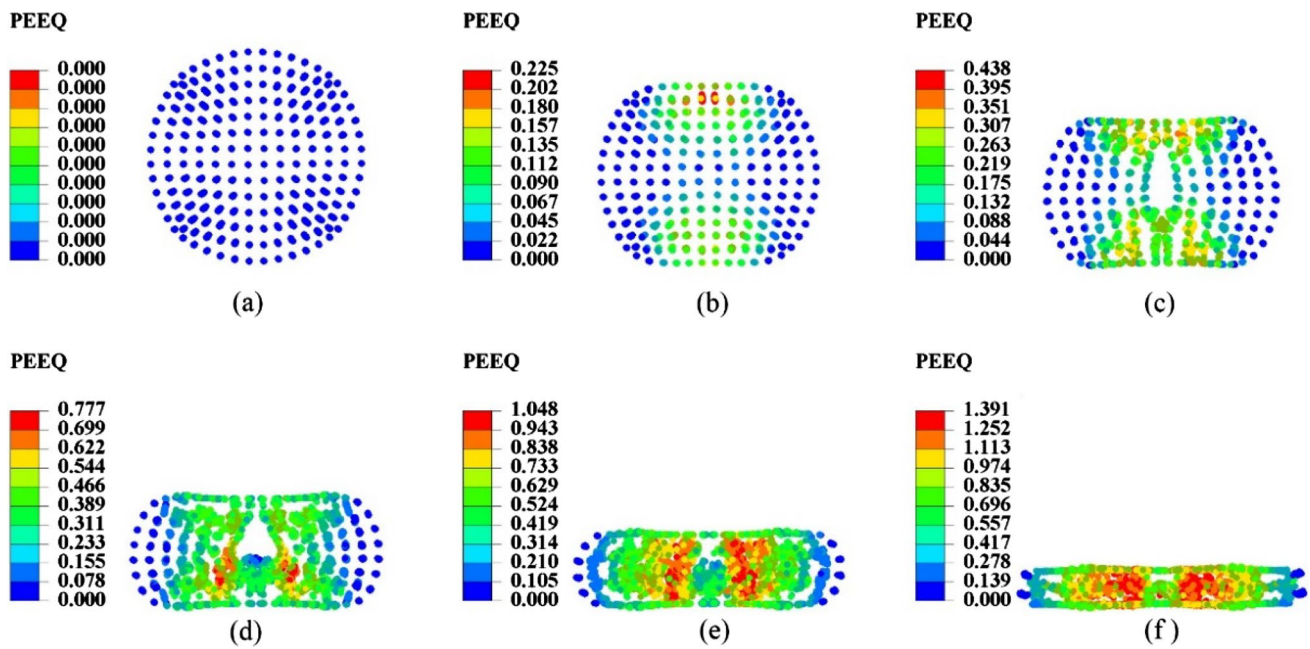


**Fig. 9** Distribution of plastic zones with different compression displacements. **a**  $s=0$  mm; **b**  $s=7$  mm; **c**  $s=14$  mm; **d**  $s=21$  mm; **e**  $s=28$  mm; and **f**  $s=35$  mm

head descends further. Foamed concrete was completely broken when the vertical compressive displacement reached 28 mm, and the vertical cracks and internal voids were completely filled with the broken concrete (e). Even though the foamed concrete at stage (f) has been completely broken, it can still be seen as a whole intact piece of concrete due to the wrapping effect of the PE pipe. At the same time, due to the significant deformation of the PE pipe, the original concentrated load has been transformed into a uniformly distributed load. The stress situation of FC-PE at this phase is similar to the unidirectional compression test of a concrete slab, and its overall stiffness has been significantly improved. Therefore, when the nominal strain reaches 60%, the dense concrete’s modulus would consequently rise sharply, quickly increasing the bearing capacity.

### 4.3 Influence of frictional properties on failure behavior of FC-PE

Clarification is required regarding the impact of the friction coefficient between the PE pipe and the foamed concrete on the loading capacity, deformation characteristics, and energy absorption effect for the numerical simulation. This method can account for the changes in the contact surface between the foamed concrete and the inner PE pipe after crushing, as opposed to creating a surface-to-surface contact. By setting the friction coefficients of foamed concrete and PE pipe to 0.2, 0.5, and 0.7, respectively, the FC-PE reaction displacement curves can be plotted using a numerical simulation

model. According to Fig. 10, the load–displacement curves nearly overlap, indicating that when the friction coefficient is changed, the reaction displacement curves of FC-PE still exhibit a three-stage trend and that the peak load and overall energy absorption essentially remain stable. It can be concluded that the friction coefficient between the foamed concrete and the PE pipe has no effect on the buffer absorber’s lateral deformation characteristics or its energy absorption state. The result illustrates that it is just necessary to inject a fixed mass of foamed concrete into the PE pipe within a set amount of time in conjunction with the production process

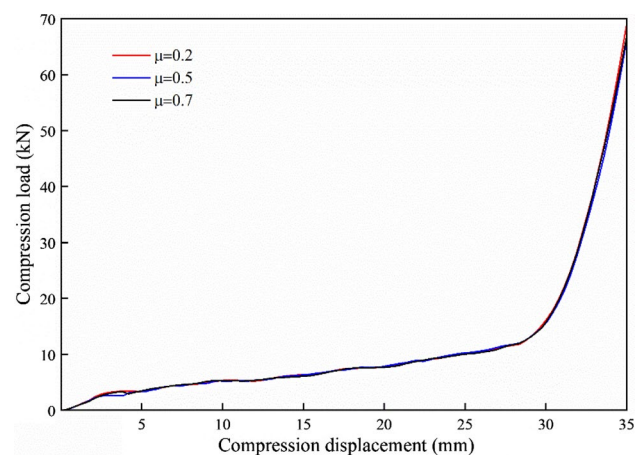


**Fig. 10** The curve of vertical reaction load–vertical displacement in different frictional properties



of filling the PE pipe with foamed concrete, with little regard for the bonding effect between the foamed concrete and the inner wall of the PE pipe. It demonstrates the theoretical underpinnings for FC-PE production process optimization, which will significantly increase FC-PE production efficiency.

#### 4.4 Influence of FC-PE size on failure behavior of FC-PE

The effect of various FC-PE sizes on the deformation characteristics and energy absorption property is investigated with the aid of the experimentally validated FEM-SPH model to simulate the mechanical behavior of foamed concrete. Various size conditions are provided in accordance with the various PE100-grade tubes on the market. Since the length of FC-PE can be viewed as a linear rise in the energy absorption condition and the PE is an isotropic material, this effect is not taken into account in this work.

As shown in Table 2, three-dimensional FC-PE numerical models of 10 diameters with various wall thicknesses were created. In order to study the effect of FC-PE diameter on the deformation of foamed concrete, the length and thickness of the PE pipe were selected as 100 and 3 mm, respectively, and various models with diameters of 40, 50, 63, 75, 90, and 110 mm were created. In the study of the FC-PE thickness on deformation characteristics and energy absorption property, the length and diameter of the PE pipe were selected as 100 and 75 mm separately and various models with thickness of 3, 4, 5, 6, and 7 mm were created. The vertical displacement of the upper plate was selected as 70% of the pipe diameter, and other model settings were the same as those shown in Fig. 5 for all models.

The compression load and displacement curves for various FC-PE diameters are shown in Fig. 11. The three-stage damage form is still present throughout the entire deformation process even though the diameters vary. The elastic phase's length nearly stays constant as the

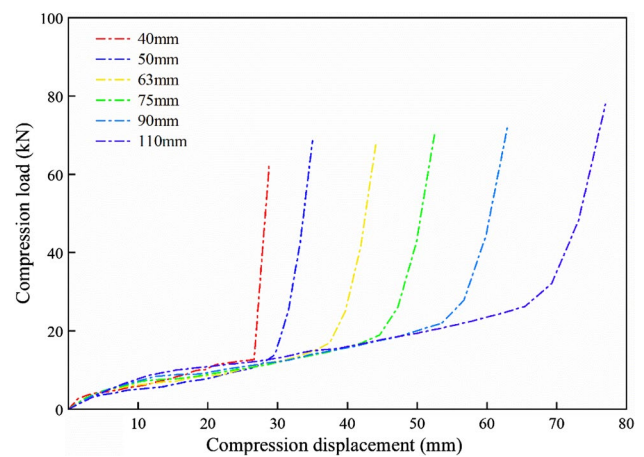


Fig. 11 The curve of vertical reaction load–vertical displacement in different diameters of FC-PE

FC-PE's diameter rises, but the elastic–plastic phase's length increases, suggesting that the deformation could be greater the larger the FC-PE's diameter. Furthermore, it shows that using thicker FC-PE does not, in practice, cause a sharp increase in the compressive load and provides better protection for tunnel concrete lining under extreme circumstances (when the nominal strain exceeds 70% of the diameter).

According to the definition of specific energy absorption, which is the amount of energy absorbed per unit mass of FC-PE, Fig. 12 shows the trend of total energy absorption (TEA) and specific energy absorption (SEA) of FC-PE under various diameter conditions. For various sizes of FC-PE, the specific energy absorption efficiency could be defined as

Table 2 Different sizes of FC-PE

No	Diameter (mm)	Thickness (mm)	Mass (g)
1	40	3	85.8
2	50	3	131.0
3	63	3	203.9
4	75	3	285.3
5	90	3	406.1
6	110	3	600.1
7	75	4	291.7
8	75	5	297.9
9	75	6	303.9
10	75	7	309.8

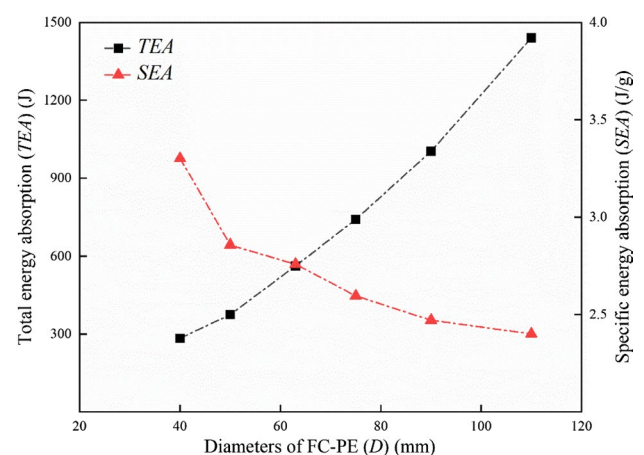
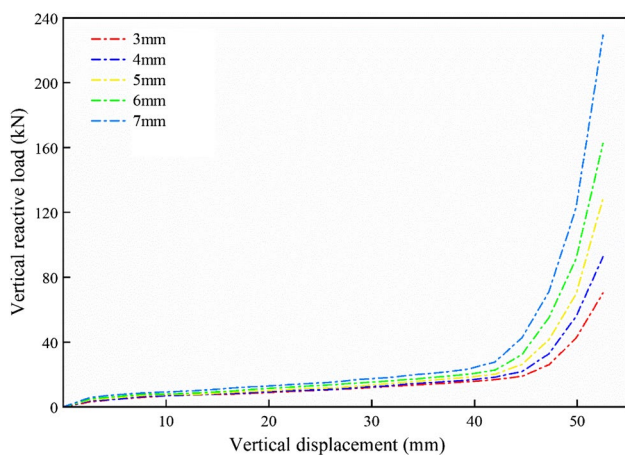


Fig. 12 Variation of the total energy absorption and specific energy absorption in different diameters of FC-PE

$$SEA = TEA/m = \int_0^s F(s)ds/m. \tag{11}$$

Due to two factors, the total energy absorption of FC-PE increases as the diameter ( $D$ ) increases: First, the larger FC-PE has a longer compression stroke, which increases the total energy absorption; second, the larger FC-PE has a larger mass of foamed concrete involved in the energy absorption under the PE wrapping, while the energy is dissipated by the four plastic hinges of the PE material. As a result of both factors, the total energy absorption increases. The specific energy absorption trend shows that there is a slight variation in specific energy absorption between different FC-PE diameters, demonstrating the stability of the energy absorber’s performance per unit volume.

Figure 13 shows the compression load and displacement curves for different thicknesses of FC-PE, which still exhibits three stages of deformation and damage during lateral compression. It indicates that with the increase in FC-PE thickness, the elastic modulus in the elastic–plastic deformation phase becomes larger and the displacement in this phase decreases. For example, the compressive displacement required for FC-PE with a pipe thickness of 7 mm to enter the compaction stage is 3 mm smaller than that of FC-PE with a pipe thickness of 3 mm. In the dense phase, the peak bearing capacity increases exponentially with the increase in the wall thickness. This is because that the FC-PE’s compression performance relies on the foam concrete’s characteristics of filling pores when concrete is broken by compression. The thicker of the pipe wall is, the less foam concrete is. The performance of the foamed concrete steadily deteriorates as wall thickness increases, and PE’s elastic–plastic hardening takes over as the dominant performance factor. It



**Fig. 13** The curve of vertical reaction load–vertical displacement in different thicknesses of FC-PE

demonstrates that both the total and specific energy absorption increase with increasing wall thickness when vertical displacement is 70% of the pipe exterior diameter. This is in conjunction with the results shown in Fig. 14.

For tunnel engineering as shown in Fig. 15, the FC-PE is compressively displaced under the action of large deformations in the soft rock, when the FC-PE is squeezed and the compressive stress is transferred to the tunnel liner. Under normal working conditions, the lining support is only used as a safety reserve, but under the action of large deformation of the soft rock, the tunnel liner needs to resist part of the stress released from the surrounding rock. FC-PE, as a proven yielding support material, is of interest to engineers for its elastic–plastic phase energy absorption properties. Therefore, the elastic–plastic phase allows the compression stroke to be of interest in study to compare the deformation and energy absorption efficiency of different sizes of FC-PE. To determine the effective yielding displacement, a function of the effective nominal strain is given as:

$$S = f(\sigma), \tag{12}$$

$$s = S_{max} = f(\sigma_0), \tag{13}$$

$$\epsilon = s/D, \tag{14}$$

where  $S$  represents the compressive displacement,  $\sigma$  represents the contact stress,  $\sigma_0$  is the maximum allowable contact stress,  $s$  represents the effective support displacement, and  $\epsilon$  is defined as the effective nominal strain.

Figure 16 shows the variation of effective yielding displacement and effective nominal strain for different diameters of FC-PE, it shows that with the increase in diameter of FC-PE, the effective yielding displacement grows from

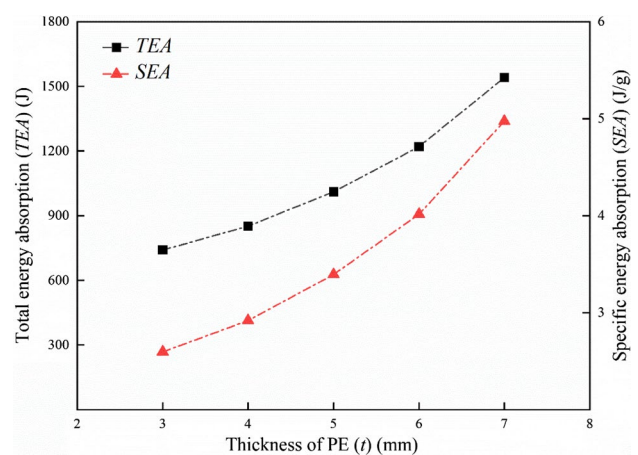


**Fig. 14** Variation of the total energy absorption and specific energy absorption in different thicknesses of FC-PE

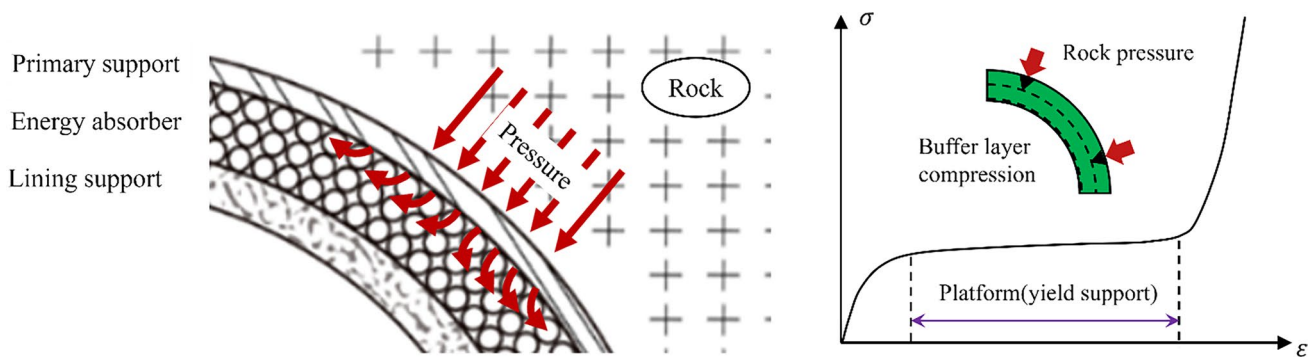


**Fig. 15** Yielding layer support structure design in rock mass

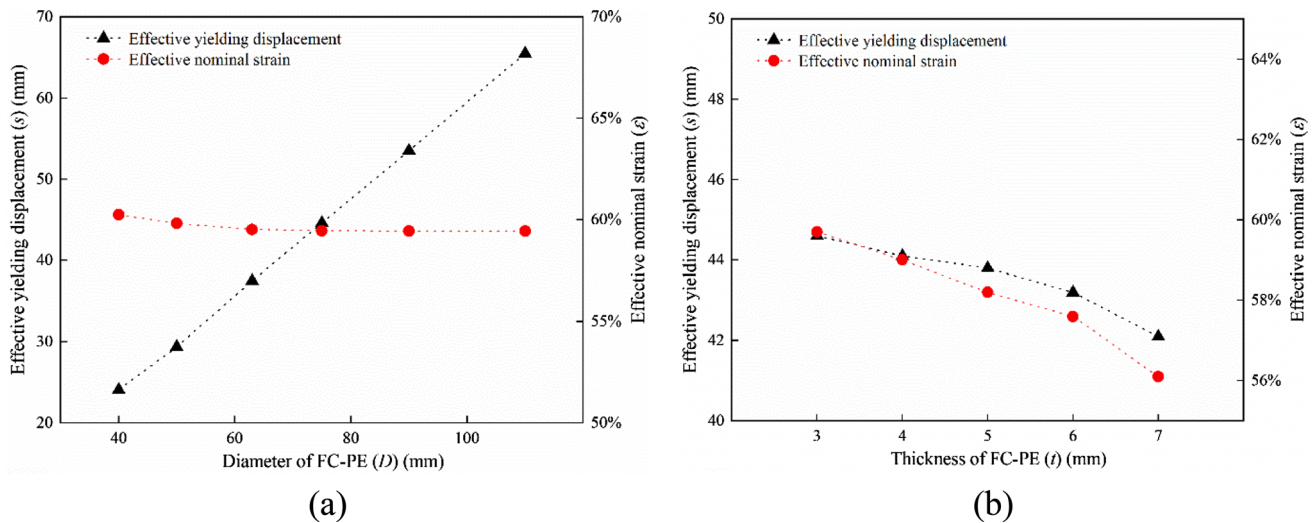


**Fig. 16** The curve of effective yielding displacement and effective nominal strain in different sizes of FC-PE: **a** diameter of FC-PE and **b** thickness of FC-PE

24 to 65 mm, and the effective yielding displacement has an approximately linear relationship with the diameter of FC-PE. It means that with the size of the FC-PE increases, the yielding support displacement would be longer and could resist more large deformation. Therefore, before construction, the size of FC-PE could be determined based on the properties of the surrounding rock mass by field investigation or numerical simulation. As far as the effective nominal strain is concerned, the diameter of FC-PE has almost no effect on the effective nominal strain. From the relationship of compression load versus compression displacement, it shows that FC-PE with larger diameter has greater energy absorption ability if the effective nominal strain is the same, and the thicker diameter FC-PE is a better selection for the yielding support structure during construction. Therefore, the large size FC-PE can be considered in the process of increasing the strength of the tunnel lining to improve the efficiency of the use of FC-PE. If increasing the wrapping thickness of FC, the effective yielding displacement and

effective nominal strain both decrease to different degrees. It also indicates that as the thickness of the pipe wall increases, the difficulty of FC-PE entering the plastic zone stage increases, and the energy absorption efficiency and deformation characteristics decrease.

### 5 Conclusion

This study established a coupled FEM-SPH numerical model for quasi-static lateral compression experiments of FC-PE and analyzed the compressive deformation properties, energy absorption properties, and damage processes of FC-PE in detail. Then, based on the numerical simulation technology, this paper investigated the influence of FC-PE's diameter (*D*), FC-PE's wall thickness (*t*), and the friction coefficient ( $\mu$ ) between foam concrete and PE pipe on FC-PE's mechanical and energy absorption characteristics. The main conclusions are drawn as follows:

- (1) The coupled FEM-SPH numerical simulation technology is suitable for simulating FC-PE's deformation process and energy absorption property when FC-PE undergoes significant deformation. The failure mode and total absorbed energy of FC-PE obtained from numerical simulation are in good agreement with the experimental results.
- (2) The deformation process of FC-PE includes three main phases: elastic stage, plastic stage, and dense stage. In the elastic stage, foam concrete and PE pipe both undergo slight deformation, and the maximum stress of foam concrete is located at the top and bottom. When the external load exceeds a certain value, foam concrete at the top and bottom breaks first and is squeezed to both sides. As the external load increases continuously, foam concrete is nearly broken completely and with the help of the PE pipe's wrapping effect, foam concrete fragments are difficult to expand freely. The FC-PE at this time is similar to a plate subjected to unidirectional compressive load in the thickness direction, causing an obvious increase in FC-PE's stiffness.
- (3) The friction coefficient ( $\mu$ ) between foam concrete and PE pipe has almost no effect on the strength and total absorbed energy of FC-PE. The total absorbed energy and strength of FC-PE both increase obviously with the increase in the pipe's diameter ( $D$ ), while the specific absorbed energy of FC-PE increases slightly with the increase in the pipe's diameter ( $D$ ). As the pipe's wall thickness ( $t$ ) increases, the total absorbed energy, specific absorbed energy, and strength of FC-PE all increase obviously. As the diameter of the FC-PE increases, the effective yield displacement increases significantly, and the energy absorption efficiency increases with the increase in diameter, while the effective nominal strain remains constant. In addition, the thickness of the PE pipe has a negative effect on the effective utilization displacement and effective nominal strain, which will reduce the energy absorption efficiency of FC-PE. The side effect of pipe diameter has a greater influence on the deformation behavior and energy absorption effect of the tube in the support of large deformation of soft rock.

**Acknowledgements** This work was supported by the National Natural Science Foundation of China (Grant Nos. 51991392 and 42293355).

**Author contributions** XC contributed to methodology, simulation, writing—original draft; XL helped in methodology, simulation, and writing—revising. XT contributed to laboratory tests on foamed concrete. DY helped in laboratory tests on PE material. HT contributed to numerical simulation. WC helped in conceptualization, supervision, and writing.

**Data availability** The data are available from the corresponding author on reasonable request.

## Declarations

**Conflict of interest** The authors declare that they have no known competing financial interests or personal relationships that could have appeared to influence the work reported in this paper.

**Ethical approval** This study was approved by the Institutional Ethics Committee of Institute of Rock and Soil Mechanics, Chinese Academy of Science. Ethics approval was not required for this research.

## References

1. Aktay L, Johnson AF, Toksoy AK, Kröplin BH, Güden M. Modeling the progressive axial crushing of foam-filled aluminum tubes using smooth particle hydrodynamics and coupled finite element model/smooth particle hydrodynamics. *Mater Des.* 2008;29(3):569–75. <https://doi.org/10.1016/j.matdes.2007.03.010>.
2. Amran YHM, Farzadnia N, Abang Ali AA. Properties and applications of foamed concrete: a review. *Constr Build Mater.* 2015;101:990–1005. <https://doi.org/10.1016/j.conbuildmat.2015.10.112>.
3. Barla G. Full-face excavation of large tunnels in difficult conditions. *J Rock Mech Geotech Eng.* 2016;8(3):294–303. <https://doi.org/10.1016/j.jrmge.2015.12.003>.
4. Barla G, Bonini M, Semeraro M. Analysis of the behaviour of a yield-control support system in squeezing rock. *Tunn Undergr Space Technol.* 2011;26(1):146–54. <https://doi.org/10.1016/j.tust.2010.08.001>.
5. Baroutaji A, Sajjia M, Olabi A-G. On the crashworthiness performance of thin-walled energy absorbers: recent advances and future developments. *Thin-Walled Struct.* 2017;118:137–63. <https://doi.org/10.1016/j.tws.2017.05.018>.
6. Bonini M, Barla G. The Saint Martin La Porte access adit (Lyon–Turin Base Tunnel) revisited. *Tunn Undergr Space Technol.* 2012;30:38–54. <https://doi.org/10.1016/j.tust.2012.02.004>.
7. Cantieni L, Anagnostou G. The interaction between yielding supports and squeezing ground. *Tunn Undergr Space Technol.* 2009;24(3):309–22. <https://doi.org/10.1016/j.tust.2008.10.001>.
8. Chen W, Tian H, Yang F, Geng Y. Study of effects of foam concrete preset deformation layer on long-term stability of deep soft rock tunnel. *Rock Soil Mech.* 2011;32:2577–83.
9. Du M, Wang X, Zhang Y, Li L, Zhang P. In-situ monitoring and analysis of tunnel floor heave process. *Eng Fail Anal.* 2020;109:104323. <https://doi.org/10.1016/j.engfailanal.2019.104323>.
10. Gao C, Zhou Z, Li Z, Li L, Cheng S. Peridynamics simulation of surrounding rock damage characteristics during tunnel excavation. *Tunn Undergr Space Technol.* 2020;97:103289. <https://doi.org/10.1016/j.tust.2020.103289>.
11. Gedikli H. Crashworthiness optimization of foam-filled tailor-welded tube using coupled finite element and smooth particle hydrodynamics method. *Thin-Walled Struct.* 2013;67:34–48. <https://doi.org/10.1016/j.tws.2013.01.020>.
12. Goel RK. Tunnelling through weak and fragile rocks of Himalayas. *Int J Min Sci Technol.* 2014;24(6):783–90. <https://doi.org/10.1016/j.ijmst.2014.10.008>.
13. He M, Guo Z. Mechanical property and engineering application of anchor bolt with constant resistance and large deformation. *Chin J Rock Mech Eng.* 2014;33:1297–308.

14. He H, Karsai A, Liu B, Hammond FL, Goldman DI, Arson C. Simulation of compound anchor intrusion in dry sand by a hybrid FEM+SPH method. *Comput Geotech.* 2023;154:105137. <https://doi.org/10.1016/j.compgeo.2022.105137>.
15. Jiang H, Zhao H, Gao K, Wang O, Wang Y, Meng D. Numerical investigation of hard rock breakage by high-pressure water jet assisted indenter impact using the coupled SPH/FEM method. *Powder Technol.* 2020;376:176–86. <https://doi.org/10.1016/j.powtec.2020.08.028>.
16. Kimura F, Okabayashi N, Kawamoto T. Tunnelling through squeezing rock in two large fault zones of the Enasan Tunnel II. *Rock Mech Rock Eng.* 1987;20(3):151–66. <https://doi.org/10.1007/BF01020366>.
17. Kimura F, Okabayashi N, Kawamoto T. Tunnelling through squeezing rock in two large fault zones of the Enasan Tunnel II. *Int J Rock Mech Min Sci Geomech Abstr.* 1988;25(2):86. [https://doi.org/10.1016/0148-9062\(88\)92141-9](https://doi.org/10.1016/0148-9062(88)92141-9).
18. Lagarón JM, López-Quintana S, Rodríguez-Cabello JC, Merino JC, Pastor JM. Comparative study of the crystalline morphology present in isotropic and uniaxially stretched “conventional” and metalocene polyethylenes. *Polymer.* 2000;41(8):2999–3010. [https://doi.org/10.1016/S0032-3861\(99\)00459-0](https://doi.org/10.1016/S0032-3861(99)00459-0).
19. Lee BJ, Argon AS, Parks DM, Ahzi S, Bartzczak Z. Simulation of large strain plastic deformation and texture evolution in high density polyethylene. *Polymer.* 1993;34(17):3555–75. [https://doi.org/10.1016/0032-3861\(93\)90039-D](https://doi.org/10.1016/0032-3861(93)90039-D).
20. Luo G, Zhao Y, Shen W, Wu M. Dynamics of bouldery debris flow impacting onto rigid barrier by a coupled SPH-DEM-FEM method. *Comput Geotech.* 2022;150:104936. <https://doi.org/10.1016/j.compgeo.2022.104936>.
21. Mardalizad A, Scazzosi R, Manes A, Giglio M. Testing and numerical simulation of a medium strength rock material under unconfined compression loading. *J Rock Mech Geotech Eng.* 2018;10(2):197–211. <https://doi.org/10.1016/j.jrmge.2017.11.009>.
22. Meng L, Li T, Jiang Y, Wang R, Li Y. Characteristics and mechanisms of large deformation in the Zhegu mountain tunnel on the Sichuan-Tibet highway. *Tunn Undergr Space Technol.* 2013;37:157–64. <https://doi.org/10.1016/j.tust.2013.03.009>.
23. Meng F, Song J, Yue Z, Zhou H, Wang X, Wang Z. Failure mechanisms and damage evolution of hard rock joints under high stress: Insights from PFC2D modeling. *Eng Anal Bound Elem.* 2022;135:394–411. <https://doi.org/10.1016/j.enganabound.2021.12.007>.
24. Moritz B. Yielding elements-requirements, overview and comparison. *Geomech Tunn.* 2011;4(3):221–36. <https://doi.org/10.1002/geot.201100014>.
25. Popov AA, Russak AV, Gladilin MP, Zaikov GY. Blends of polypropylene and high density polyethylene. *Polym Sci USSR.* 1986;28(5):1208–15. [https://doi.org/10.1016/0032-3950\(86\)90273-X](https://doi.org/10.1016/0032-3950(86)90273-X).
26. Rodríguez R, Díaz-Aguado MB. Deduction and use of an analytical expression for the characteristic curve of a support based on yielding steel ribs. *Tunn Undergr Space Technol.* 2013;33:159–70. <https://doi.org/10.1016/j.tust.2012.07.006>.
27. Tan X, Chen W, Liu H, Chan AHC, Tian H, Meng X, Deng X. A combined supporting system based on foamed concrete and U-shaped steel for underground coal mine roadways undergoing large deformations. *Tunn Undergr Space Technol.* 2017;68:196–210. <https://doi.org/10.1016/j.tust.2017.05.023>.
28. Tian H, Chen W, Tan X, Tian Y, Zhang N. Investigating polymeric foam materials as compressible layer for tunnelling in squeezing ground conditions. *Tunn Undergr Sp Technol.* 2022;122:104391. <https://doi.org/10.1016/j.tust.2022.104391>.
29. Wang FN, Guo ZB, Qiao XB, Fan JY, Li W, Mi M, et al. Large deformation mechanism of thin-layered carbonaceous slate and energy coupling support technology of NPR anchor cable in Minxian Tunnel: a case study. *Tunn Undergr Space Technol.* 2021;117:104151. <https://doi.org/10.1016/j.tust.2021.104151>.
30. Wang W, Wu Y, Wu H, Yang C, Feng Q. Numerical analysis of dynamic compaction using FEM-SPH coupling method. *Soil Dyn Earthq Eng.* 2021;140:106420. <https://doi.org/10.1016/j.soildyn.2020.106420>.
31. Wang J, Zhang Y, Qin Z, Song S, Lin P. Analysis method of water inrush for tunnels with damaged water-resisting rock mass based on finite element method-smooth particle hydrodynamics coupling. *Comput Geotech.* 2020;126:103725. <https://doi.org/10.1016/j.compgeo.2020.103725>.
32. Windsor CR, Thompson AG. 16—Rock reinforcement—technology, testing, design and evaluation. In: Hudson JA, editor. *Excavation, support and monitoring.* Turkey: Pergamon; 1993. p. 451–84.
33. Wu H, Fan F, Yang X, Wang Z, Lai J, Xie Y. Large deformation characteristics and treatment effect for deep bias tunnel in broken phyllite: a case study. *Eng Fail Anal.* 2022;135:106045. <https://doi.org/10.1016/j.engfailanal.2022.106045>.
34. Xiang Y, Wang M, Yu T, Yang L. Key performance indicators of tubes and foam-filled tubes used as energy absorbers. *Int J Appl Mech.* 2015;07(04):1550060. <https://doi.org/10.1142/S175882511550060X>.
35. Xu G, He C, Yang Q, Wang B. Progressive failure process of secondary lining of a tunnel under creep effect of surrounding rock. *Tunn Undergr Space Technol.* 2019;90:76–98. <https://doi.org/10.1016/j.tust.2019.04.024>.
36. Yang J, Chen W, Yang D, Yuan J. Numerical determination of strength and deformability of fractured rock mass by FEM modeling. *Comput Geotech.* 2015;64:20–31. <https://doi.org/10.1016/j.compgeo.2014.10.011>.
37. Yu W, Wang B, Zi X, Guo X, Wang Z. Effect of prestressed anchorage system on mechanical behavior of squeezed soft rock in large-deformation tunnel. *Tunn Undergr Space Technol.* 2023;131:104782. <https://doi.org/10.1016/j.tust.2022.104782>.
38. Zhang ZD. Discussion and study on large deformation of tunnel in squeezing ground, 5–12+40 modern. *Tunn Technol.* 2003. <https://doi.org/10.13807/j.cnki.mtt.2003.02.002>.
39. Zhang R, Chen G, Zou J, Zhao L, Jiang C. Study on roof collapse of deep circular cavities in jointed rock masses using adaptive finite element limit analysis. *Comput Geotech.* 2019;111:42–55. <https://doi.org/10.1016/j.compgeo.2019.03.003>.
40. Zhang C, Tan X, Tian H, Chen W. Lateral compression and energy absorption of foamed concrete-filled polyethylene circular pipe as yielding layer for high geo-stress soft rock tunnels. *Int J Min Sci Technol.* 2022;32(5):1087–96. <https://doi.org/10.1016/j.ijmst.2022.08.011>.
41. Zhou Z, Zhang D, Gao C, Li Z, Li M, Liu G. A PD-FEM approach for fast solving static failure problems and its engineering application. *Eng Fract Mech.* 2022;262:108269. <https://doi.org/10.1016/j.engfracmech.2022.108269>.

**Publisher's Note** Springer Nature remains neutral with regard to jurisdictional claims in published maps and institutional affiliations.

Springer Nature or its licensor (e.g. a society or other partner) holds exclusive rights to this article under a publishing agreement with the author(s) or other rightsholder(s); author self-archiving of the accepted manuscript version of this article is solely governed by the terms of such publishing agreement and applicable law.